10th International Conference on Fracture Mechanics of Concrete and Concrete Structures
FraMCoS-X
G. Pijaudier-Cabot, P. Grassl and C. La Borderie (Eds)
https://doi.org/10.21012/FC10.233601

DEM INVESTIGATIONS OF EFFECT OF INTERFACIAL TRANSITION ZONES ON CONCRETE FRACTURE

MICHAŁ NITKA* **AND JACEK TEJCHMAN***

* Gdańsk University of Technology, Gdańsk
Narutowicza 11/12, 80-233 Gdańsk, Poland
e-mail: tejchmk@pg.edu.pl

Key words: aggregate, concrete beam, DEM, fracture, interfacial transition zones, x-ray μCT

Abstract: The paper presents two-dimensional numerical mesoscopic results for concrete at the aggregate level in a notched concrete beam under bending. A classical particle discrete element method was used to predict both concrete strength and fracture. A 4-phase concrete description including aggregate, cement matrix, macro-voids and interfacial transition zones (ITZs) was used to take heterogeneity into account. ITZs were simulated as porous zones around aggregates with a defined width and the same mechanical properties as the cement matrix. The model was calibrated based on experiments and x-ray μCT scans. Attention was laid on both the effect of initial micro-porosity in ITZs on the load-deflection curve and shape of a discrete macro-crack. The findings presented in this paper can offer a new perspective as to the understanding of the micro-cracking development in concrete.

1 INTRODUCTION

Concrete is generally referred to as a heterogeneous and discontinuous material that may be considered at the meso-scale as a composite material wherein four germane phases (constituents) may be isolated: cement paste, aggregate, macro-voids and interfacial transition zones (ITZs) between aggregates cement paste. ITZs reveal pronounced compositional differences as compared to the cement paste. Those differences are the strongest in the immediate vicinity of aggregates' surfaces and gradually diminish away from aggregates to become insignificant at a certain distance (15-100 μm) [1]-[4]. In general, ITZs contain more and larger pores, smaller particles and higher porosity, less anhydrous cement and (calcium silicate hydrate, C-S-H) gel, resulting in higher transport properties (i.e., permeability, diffusivity and conductivity) in contrast to the cement paste [5], [6]. ITZs facilitate ingress and movement external aggressive agents into concrete (water and harmful ions easily penetrate into concrete resulting in the deterioration of both concrete and reinforcement). The presence of highly porous heterogeneous ITZs in concrete is thus crucial from the mechanical point of view, since they are always the weakest regions in usual concretes due to their higher porosity and thus govern the global strength. They become also attractors for a macro-crack as a weak link that evolves by bridging interfacial micro-cracks [7]. ITZs stem from the wall effect of packing of cement grains against the relatively flat aggregate surface which disrupts the packing of cement grains and is responsible for the features of ITZs, particularly for their higher porosity [3]. Another origin of ITZs is a micro-bleeding effect where ITZs accumulate free water around aggregates, especially under large aggregates, and increases the local porosity. ITZs are believed to be affected by many factors, such as particle diameter, water/cement ratio, aggregate texture, aggregate roughness, aggregate size

distribution and curing age. In order to take ITZs into account in calculations, the mesoscopic models have to be used at the aggregate level. They can be based on finite element (FE) models using different enhanced constitutive laws and discrete models [7], [9]. ITZs were always simulated as zones with a defined or zero width and possessing the reduced stiffness and strength as compared to the cement matrix.

Our research works are aimed at formulating a realistic 3D multi-scale mechanical model for concrete to optimize its strength and fracture properties, based both on strength laboratory experiments and x-ray μCT images using very advanced micro-tomography system [10]. The numerical model could replace (by changing several factors at the same time) costly experimental tests to elaborate quantitative recommendations for the optimum aggregate volume content, aggregate shape and roughness and mortar macro-porosity in concrete (to simultaneously obtain both the relatively high strength and ductility of concrete). The effect of fibres and additional grains of different syntactic foams as e.g. glass and polymer micro-spheres, cement hollow spheres on the concrete behaviour might be also taken into account that would lead to a better design of concrete mixes with respect to strength and ductility.

2 IN-HOUSE EXPERIMENTS

The laboratory tests using x-ray micro-computed tomography with two simply supported notched concrete beams subjected to quasi-static three-point bending were described in [7]. The rectangular beam cross-section had the height of H=80 mm and width of B=40 mm. The beam's total length was L=320 mm (4×H) and the span between the supports was 3×H=240 mm. A macro-crack was triggered in the beam's mid-part by a notch whose height was H/10=8 mm and the width of 3 mm. The concrete mixture was composed of round-shape gravel aggregate and sand grains (maximum particle diameter d_{max}=16 mm, mean particle diameter d_{50}=2 mm), Portland cement (CEM I 32.5 R) and water. The total particle (aggregate and sand) volumetric content was V=75%. The total aggregate content with the diameter equal to or larger than 2 mm was V=37%. The initial micro-porosity of concrete was about 5% [10]. The tests were performed with a constant-controlled notch opening displacement rate of 0.002 mm/min (crack mouth opening displacement (CMOD)) using the loading machine Instron 5569.

The distribution of aggregate and macro-voids in the concrete beams was determined based on μCT images of concrete cuboids (80×50×40 mm^3) extracted from the mid-part of each beam after the tests [11]. Figure 2D shows 3D images of the concrete internal structure obtained with the aid of the x-ray micro-tomography system SkyScan 1173 that represents a new generation in high-resolution desktop micro-computed tomography systems. This micro-CT system was described in detail in [10]. The main discrete macro-crack was strongly curved along the beam height and width due to a random presence of aggregate grains (Fig.1).

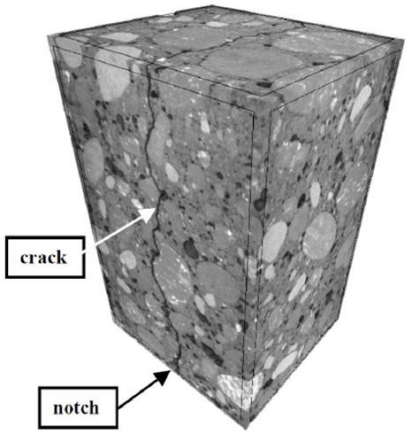

Figure 1: X-ray μCT image of cracked cuboidal specimens 80×50×40 mm^3 cut out from beam pull-out.

It was created above the notch and propagated upwards due to bending. It mainly moved through the weakest phase in concrete that were ITZs. Thus, micro-cracking was first activated in ITZs and when two interfacial cracks occurred around adjacent aggregates, a crack inside the cement matrix initiated to bridge the interfacial cracks so that a connected

crack path was formed. Sometimes the crack propagated through macro-voids and very rarely through a single weak aggregate grain [10]. A very non-uniform porous structure of ITZs and the presence of separated small sand grains was possible to be observed with the maximum magnification factor of 30 000 using scanning electro-microscope (SEM) Hitachi TM3030. The width of porous ITZs on the concrete surface did not depend on aggregate particle diameter and changed between 30-50 μm (Fig.2a). ITZs appeared around all aggregate grains (d_a≥2 mm) and usually covered about 80-90% of the aggregate circumference that was probably caused by a formation of water lenses beneath aggregate grains during mixing [3]. The experimental porosity of ITZs changed between 25% (at aggregates) down to 5% (cement matrix), based on the image binarization technique (Fig.2). From the digital image of ITZ, a white-black bitmap was first created wherein the black colour corresponded to porous and white colour to aggregate and cement matrix. Next, the width of ITZ was divided into strips of the aggregate shape 5 μm wide and the black and white pixels were calculated. The porosity of each strip was determined as the percentage of the area of pores to total strip area.

3 DEM MODEL

Outstanding advantages of DEM include its ability to explicitly handle the modelling of particle-scale properties including size and shape which play an important role in the concrete fracture behaviour [7]. The 3D spherical discrete element model YADE takes advantage of the so-called soft-particle approach (i.e. the model allows for particle deformation which is modelled as an overlap of particles) [12-13]. Aggregate grains were modelled as clusters composed of spheres. A linear normal contact model under compression was used. The interaction force vector representing the action between two spherical discrete elements in contact was decomposed into the normal and tangential components. A cohesive bond was assumed at the grain contact exhibiting brittle failure under the critical normal tensile load. The tensile failure initiated contact separation and the shear cohesion failure initiated contact slip and sliding obeying the Coulomb friction law under normal compression. The detailed model description and calibration procedure was described in [7], [11], based on real simple standard laboratory tests (uniaxial compression and uniaxial tension) of concrete specimens.

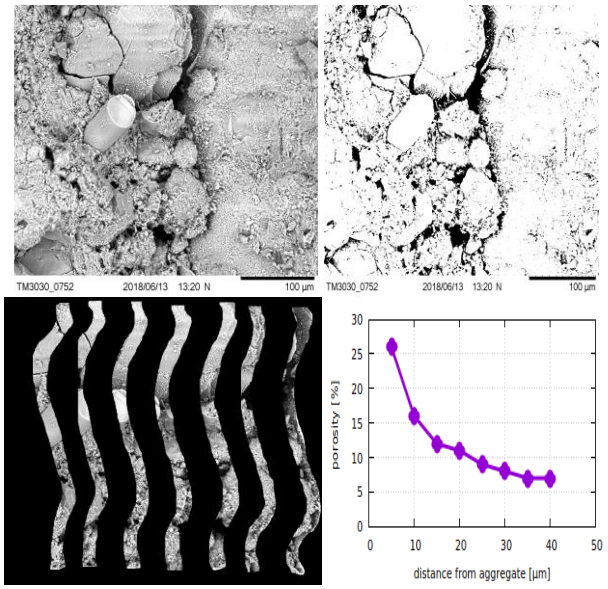

Figure 2: ITZ strips moved successively starting from aggregate surface towards cement matrix and porosity change in ITZ versus distance from aggregate based on binarization technique.

At the meso-scale concrete was described in DEM computations (beam mid-region only, Fig.3a) as a four-phase material composed of aggregate, cement matrix, ITZs and macro-voids. The numerical analyses were performed on one concrete beam with the same aggregate location and shape as in the experiment with the aid of μCT-images [11]. In 2D calculations, the beam thickness included one row of aggregate and mortar particles. All aggregates in the beam (2 mm≤d_a≤16 mm) were modelled as grain clusters connected to each other. One aggregate particle depending upon its diameter included from 2 up to 300. All aggregate grains with d_a≥2 mm included porous ITZs. The spherical elements were solely assumed in the cement matrix (0.25 mm≤ d_{cm} <1 mm) without ITZs. The global initial micro-porosity of the cement matrix was 5% that

corresponded to the real concrete compactness. To reduce the computation time, the thickness of ITZs was assumed as 0.75 mm (≈3 rows of spheres) (Fig.3b). The micro-porosity of ITZs was assumed as $p_{(ITZ)}$=5%, 7%, 10%, 15%, 20% and 25%. The macro-voids (only with the diameter d_{mv}≥1 mm) were modelled as the empty regions of a real shape [11].

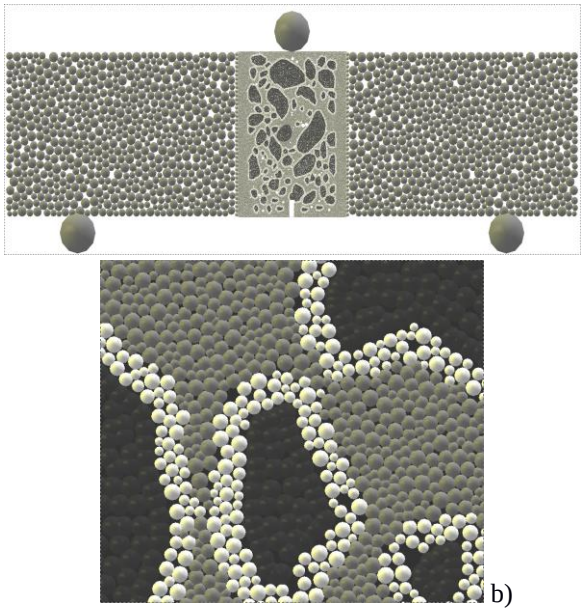

Figure 3: Geometry of concrete beam model in DEM: a) front side of the entire beam and b) zoom into ITZ layers (dark grey corresponds to aggregate, grey colour to cement matrix and light grey colour to ITZs).

The following parameters were used for the calculations in all DEM analyses for the cement matrix: elastic modulus of particle contact $E_{c,cm}$=16.8 GPa, Poisson's ratio of particle contact ν_c=0.2, cohesive stress C_{cm}=180 MPa and tensile normal stress T_{cm}=28 MPa (C_{cm}/T_{cm}=5.5). The remaining parameters were equal to μ=18º (inter-particle friction angle) and ρ=2600 kg/m^3 (mass density of concrete). The above listed DEM parameters were calibrated with the aid of calculations of 2D uniaxial compression tests for mortar and concrete.

4 DEM RESULTS

Figure 4 shows the numerical global curves of the resultant vertical force versus CMOD with the different initial micro-porosity $p_{(ITZ)}$ of ITZs as compared to one experimental outcome for the vertical cross-section of the beam mid-region at the depth of 10 mm from the front side. The calculated maximum vertical force from 2D DEM obviously decreased with increasing micro-porosity of ITZs $p_{(ITZ)}$. It was e.g. F_{max}=2.85 kN (CMOD=0.020 mm) for $p_{(ITZ)}$=0% and F_{max}=1.9 kN (CMOD=0.018 mm) for $p_{(ITZ)}$=25%. The concrete brittleness decreased with increasing $p_{(ITZ)}$. The best agreement with the experiment was achieved for $p_{(ITZ)}$=20% with respect to the strength and ductility. The effect of $p_{(ITZ)}$ proved to be strong. With the real significantly lower width of ITZs, the effect of $p_{(ITZ)}$ would be smaller.

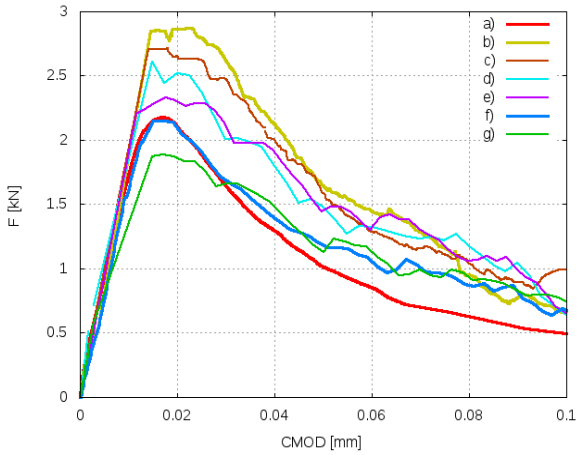

Figure 4: Evolution of global vertical force F against CMOD in beam under 3-point bending: 2D DEM curves with different initial micro-porosity of ITZ $p_{(ITZ)}$ (b) 5%, c) 7%, d) 10%, e) 15%, f) 20% and g) 25%) as compared to experimental curve (a).

The final crack path in the region above the notch (in red) is described in Fig.5. The final crack was more curved with increasing $p_{(ITZ)}$. For $p_{(ITZ)}$=15%-25% its shape was similar as in the experiment.

5 CONCLUSIONS

The detailed 2D analyses were conducted to examine a particle-scale response during the deformation process to elucidate the micro-cracking evolution in ITZs responsible for the macroscopic properties. Our numerical 2D mesoscopic approach based on the discrete element method and x-ray μCT images for the characterisation of a quasi-static mechanical behaviour of concrete was able to predict the

progressive nature of concrete cracking from the mesoscopic to the macroscopic level. It demonstrated a close correlation between numerical and experimental results in terms of strength and fracture propagation across macroscopic and particle scales.

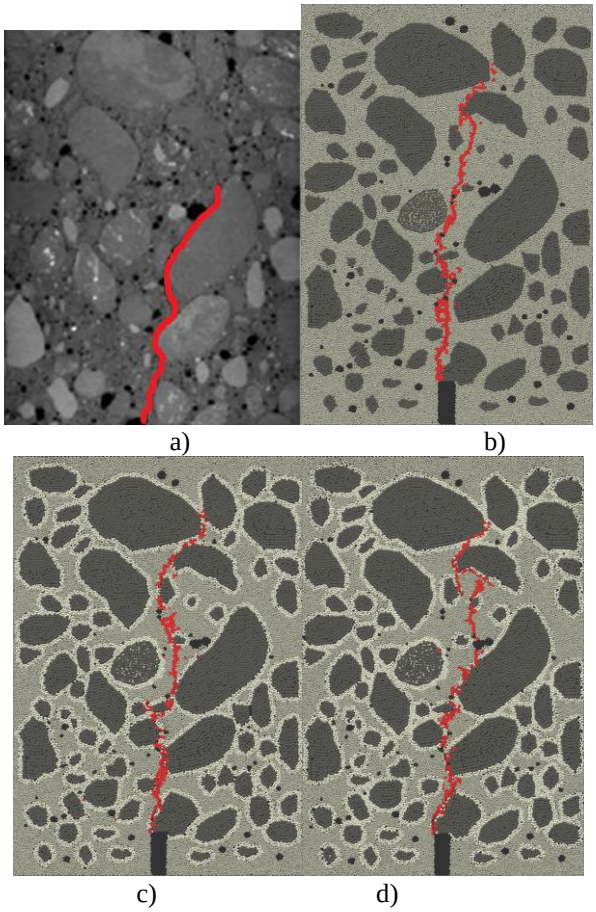

Figure 5: Final crack trajectory in concrete beam above notch after test a) from x-ray μCT-scan at depth of 10 mm from beam front side and from 2D DEM with initial micro-porosity of: b) $p_{(ITZ)}$=5% (no ITZ), c) $p_{(ITZ)}$=10% and d) $p_{(ITZ)}$=20% (red colour denotes broken contacts, dark grey denotes aggregate, grey denotes cement matrix, light grey denotes ITZ and black colour denotes macro-voids).

The effect of initial micro-porosity in ITZs on the beam response was pronounced. The beam strength and stiffness increased with decreasing micro-porosity of ITZs. The beam brittleness became smaller with increasing micro-porosity ITZs. The macro-crack curvature increased with increasing micro-porosity of ITZs.

Our improved DEM model may be next connected to the computational fluid dynamics (CFD) to study global and local problems of the heat and humidity transport in concrete [14].

Acknowledgements

The research work has been carried out within the project ‘‘*Innovative ways and effective methods of safety improvement and durability of buildings and transport infrastructure in the sustainable development*” financed partly by the European Union POIG.01.01.02-10-106/09-01) and the project ‘‘*Fracture propagation in rocks during hydro-fracking - experiments and discrete element method coupled with fluid flow and heat transport*” financed by the National Science Centre (NCN) (UMO-2018/29/B/ST8/00255).

REFERENCES

[1] Bentz, D.P., Stutzman, P.E. and Garboczi, E.J., 1992. Experimental and Simulation Studies of the Interfacial Zone in *Concrete. Cem. and Conc. Res.* **22**(5):891.

[2] Scrivener K.L. and Nemati K.M., 1996. The percolation of pore space in the cement paste/aggregate interfacial zone of concrete. *Cem. and Conc. Res.* **26**:35-40.

[3] Scrivener K.L., Crumbie A.K. and Laugesen P., 2004. The interfacial transition zone (ITZ) between cement paste and aggregate in concrete, *Interface Sci*. **12**:411-421.

[4] Bentur A. and Alexander M.G., 2000. A Review of the Work of the RILEM TC 159-ETC: Engineering of the Interfacial Transition Zone in Cementitious Composites. *Mat. and Struc.* **33**(2): 82-87.

[5] Li K., Stroeven P, Stroeven M. and Sluys L. J., 2017. A numerical investigation into the influence of the interfacial transition zone on the permeability of partially saturated cement paste between aggregate surfaces. *Cem. and Conc. Res.* **102:**99-108.

[6] Li K., Stroeven P, Stroeven M. and Sluys L. J., 2017. Effects of technological parameters on permeability estimation of partially saturated cement paste by a DEM

approach. *Cem. and Conc. Comp.* **84**: 222-231.

[7] Nitka M. and Tejchman J., 2018. A three-dimensional meso scale approach to concrete fracture based on combined DEM with X-ray μCT images. *Cem. and Conc. Res.* **107**:11-29.

[8] Lagerblad B and Kjellsen K.O., 1999. Normal and high strength concretes with conventional aggregates. Engineering and transport properties of the interfacial transition zone in cementitious composites – state-of-the-art report of RILEM TC 159-ETC and 163-TPZ. *RILEM Publications* SARL:53-70.

[9] Suchorzewski J, Tejchman J. and Nitka M.,2018. Discrete element method simulations of fracture in concrete under uniaxial compression based on its real internal structure, *Int. J. of Damage Mech.* **27**(4):578-607.

[10] Skarzynski Ł. and Tejchman J., 2016. Experimental investigations of fracture process in concrete by means of x-ray micro-computed tomography, *Strain* **52**:26-45.

[11] Skarżyński Ł., Nitka M. and Tejchman J., 2015. Modelling of concrete fracture at aggregate level using FEM and DEM based on x-ray μCT images of internal structure, *Eng. Frac. Mech.* **10**(147):13-35.

[12] Kozicki J. and Donzé F.V., 2008. A new open-source software developer for numerical simulations using discrete modeling methods, *Comp. Met. in Applied Mech. and Engi.* **197**:4429-4443.

[13] Šmilauer V. and Chareyre B., 2011. Yade DEM Formulation. Manual.

[14] Krzaczek M., Kozicki J., Nitka M. and Tejchman J. Simulations of hydro-fracking in rock mass at meso-scale using fully coupled DEM/CFD approach. *Acta Geotechnica*, doi: 10.1007/s11440-019-00799-6, 2019.